Langmuir

Article

pubs.acs.org/Langmuir

Influence of Induced-Charge Electrokinetic Phenomena on the Dielectrophoretic Assembly of Gold Nanoparticles in a Conductive-Island-Based Microelectrode System

Haitao Ding, Weiyu Liu, Jinyou Shao,* Yucheng Ding, Liangliang Zhang, and Jiqiang Niu

Micro- and Nano-manufacturing Research Center, State Key Laboratory for Manufacturing Systems Engineering, Xi'an Jiaotong University, Xi'an, Shaanxi 710049, China

ABSTRACT: Metal nanoparticles in a liquid suspension can be assembled dielectrophoretically (DEP) into nanoparticle chains, which can serve as electrical functional microwires connecting isolated and conductive elements to an electrode pair, as used in wet electronics, bioelectronics, and biochemical sensors. The frequency-dependent morphology of these nanoparticle chains assembled between an electrode pair has even been attributed to the decreasing magnitude of alternating current electroosmosis (ACEO) flow velocity with driving frequency. For instance, highly oriented nanoparticle nanowires can be generated by DEP assembly only at a high frequency, which induces a negligible small ACEO above the electrode surface, corresponding to fewer nanoparticles transported to the assembly region. In this study, attention is focused on the formation of nanoparticle chains in a conductive-island-based microelectrode system. It is worth noting that the intrusion of an island entity can bring about further double-layer polarization and induced charge electroosmosis flow (ICEO) around this conductive object, which exerts a significant influence on DEP assembly. In our experiments, the ends of nanoparticle chains are always extended onto the metal surfaces at 50 kHz, and their central parts become slender at 150 kHz. Meanwhile, wire-shaped particle clusters aligned along the direction of local field lines are more densely distributed at the island rims than that growing from the electrode edges. Consequently, a series of numerical modeling based on the theory of induced charge electrokinetic phenomena are introduced to account for these regular experimental results, including the double-layer charging effect at the metal/electrolyte interface, ACEO, ICEO, and electrothermal flow. Mutual DEP is also treated as an important factor affecting DEP behavior when neighboring particles are approaching one another. The results from the theoretical study are in good agreement with the experimental observations.

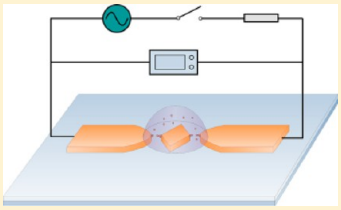

1. INTRODUCTION

One of the major challenges in nanotechnology is the formation of connections and interfaces among a series of small elements in wet electronic and bioelectronic circuits.[1,2] Dielectrophoresis (DEP) has been proved to be a convenient way to manipulate and separate microscale or nanoscale objects such as nanoparticles,[3−8] nanowires,[9,10] carbon nanotubes,[11,12] DNA,[13,14] cells,[15−18] and virus.[19] Metal nanoparticles can be assembled in situ from a liquid suspension into microwire electrical connections in the form of pearl chains by DEP. Gold nanoparticle chains bridging the opposing electrode tips, where the electric field is most intensive, often have good ohmic conductance, as has been proven by some pioneering researchers.[2,20]

It has been reported that the morphology of pearl chain formations (PCF) is susceptible to the driving frequency of the alternating current (ac) voltage signal applied to the electrode pair in that they become thinner and more highly oriented along the direction of local electric field lines with frequency.[6,7] This discovery was mostly attributed to diminishing ac electroosmosis (ACEO) convective flows at high frequencies, leading to a decreased number of nanoparticles transported into the assembly region and a weakened perturbation of ACEO flow to DEP-driven force.[6,7]

Hermanson et al. have demonstrated in an experiment that DEP-assembled gold nanoparticle chains can spontaneously form microwire electrical connections to an individual carbon island located in the gap between a coplanar electrode pair.[2] Later, Bhatt and Velev successfully made a discrimination of two distinct assembly modes in the course of PCF (i.e., bulk and surface assembly modes[20]). Moreover, they put forward the concept of a "conductive island" that is enclosed in the isolation spacing in a deliberate manner so as to make an adjustment in the growth direction of nanoparticle chains. The wire growth starts at the island as a result of a local field intensification around this conductive object. Consequently, nanoparticle chains tend to connect spontaneously to the island and finally grow an electrical circuit network in the liquid phase. Their work points the way for nanotechnology applications that demand the formation of electrical connections between nanodevices in the framework of wet electrical circuits.

Although PCF in the presence of a conductive object has been explored, it still requires an in-detail investigation of the frequency-dependence assembly in such systems. Besides, severe double-layer polarization around the conducting island

Received: May 29, 2013
Revised: August 2, 2013
Published: September 2, 2013

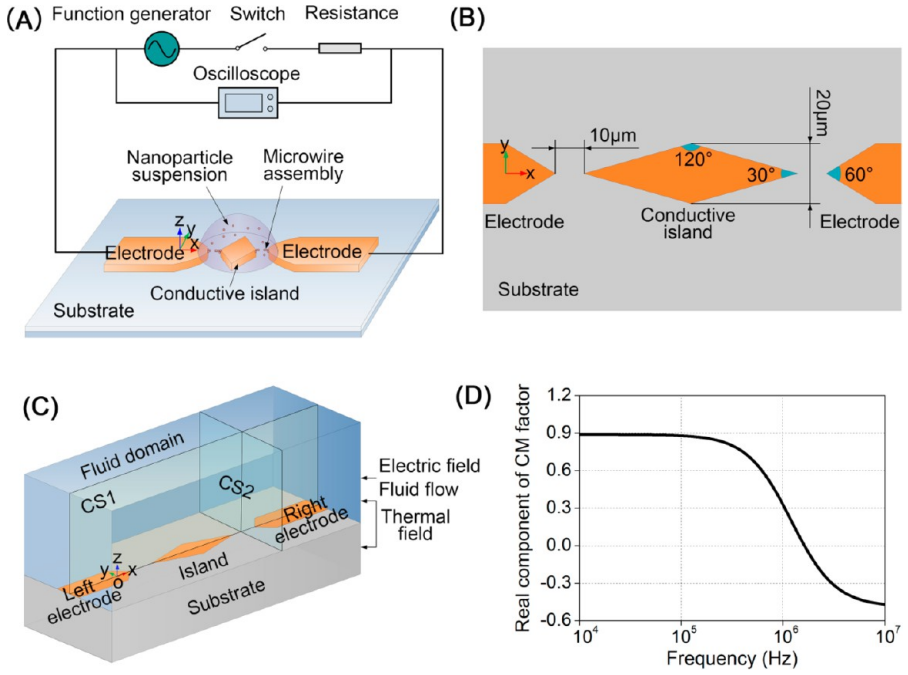

Figure 1. (A) Schematic representation of the experimental setup used in the DEP-directed superassembly of gold nanoparticles in a conductive-island-based microelectrode system. (B) Illustration of the size and geometric configuration of the conductive objects. (C) Computational domain of the electric field, thermal field, and fluid dynamics in the numerical simulation (not to scale). Cross section 1 (CS1) indicates the symmetrical $x-z$ cross section, and cross section 2 (CS2) denotes the $y-z$ cross section in the assembly region. (D) Real part of the CM factor of the 10 nm gold nanoparticle with respect to its suspending medium as a function of driving frequency.

at low frequencies has the potential to cause convective rolls over the island surface in the form of induced charge electroosmosis (ICEO) flow,[21] which can have a significant effect on PCF assembly.

In this article, we designed a specific conductive-island-based microelectrode system, and an experimental and theoretical study concerning the influence of the conductive object on PCF was carried out. It is worth noting that the intrusion of the island entity brings about further double layer polarization as well as additional electrokinetic fluid rolls as a result of an uneven electric field distribution around this conductive object. Consequently, the theory of induced charge electrokinetic phenomena (ICEK) is introduced here to account for the various regular experimental observations, such as the capacitive charging of the electrical double layer (EDL) at the metal/electrolyte interface (metal includes the electrode as well as the conductive island), ACEO and ICEO fluid flows, and a bulk flow effect due to induction electrohydrodynamics (EHD).

Besides, when neighboring particles are approaching one another, mutual DEP is also treated as an important factor affecting their movement.

2. EXPERIMENTAL SECTION

A DEP experiment is conducted in a conductive-island-based electrode system. The fabrication of the DEP device is based on a standard silicon micromachining process. The metallic electrodes mounted on an insulating SiO_2 substrate are composed of a 10-nm-thick chromium layer used for adhesion enhancement and a 90-nm-thick gold layer deposited on the chromium required by electrical conductance. In this work, a colloidal suspension of gold nanoparticles with 10 nm diameter was used, which is commercially available from BBI (British Biocell International). After a droplet of the gold nanoparticle suspension was dripped to cover the electrode gap, a harmonic voltage signal with an amplitude of 10 V and a driving frequency varying from 50 to 500 kHz was applied to the microelectrode pair using a function generator (Agilent 33220A) by needle probes (Wentworth Laboratories MP1008). The voltage drop between the two probes was monitored with an oscilloscope (Tektronix DPO3034). When a complete nanoparticle chain assembled by DEP bridges the electrodes and island, there is a sharp jump in the voltage drop monitored in the oscilloscope, which serves as a trigger to switch off the function generator immediately. Then the sample was washed in deionized water and dried with a slow stream of nitrogen gas flow.

Figure 1A,B shows the experimental setup design used in the study of nanoparticle self-assembly, where a pair of sharp-tipped electrodes and a diamond-shaped conductive island are utilized. The closest distance between one electrode and the island is 10 μm, and their width is 20 μm.

3. THEORETICAL BASIS

3.1. Interfacial Charge Relaxation and Dielectrophoresis. At driving frequencies below several hundred megahertz, through Maxwell–Wagner interfacial polarization, Coulomb force acting on the induced charge at the interface of two materials of different electric properties will transport the medium of more polarizability to regions of largest field intensity and vice versa.

For a spherical particle of radius R immersed in a liquid suspension of dielectric constant ε_f and under a background electrical field $\boldsymbol{E}$ with no spatial phase variation, the time-averaged dielectrophoretic force acting on the rigid body can be approximated using the point dipole model

$$\langle \mathbf{F}_{DEP} \rangle = \pi \varepsilon_f R^3 Re[f_{CM}(\omega)] \nabla (\tilde{\mathbf{E}} \cdot \tilde{\mathbf{E}}^*) \quad (1)$$

Here, $\tilde{\mathbf{E}}$ is the phasor amplitude of the electric field vector (i.e., $\mathbf{E} = Re(\tilde{\mathbf{E}} e^{j\omega t})$, ω the angular frequency of the applied ac signal, and * is the operator of the complex conjugate.

The frequency dependence of the DEP force consists of the Clausius–Mossotti (CM) factor $f_{CM}(\omega)$, especially for a particle of spherical shape

dx.doi.org/10.1021/la402060g | Langmuir 2013, 29, 12093–12103

$$f_{CM}(\omega) = \frac{\tilde{\varepsilon}_p - \tilde{\varepsilon}_f}{\tilde{\varepsilon}_p + 2\tilde{\varepsilon}_f} \quad (2)$$

Here, subscripts p and f represent the particle and fluid, respectively. $\tilde{\varepsilon}_i = \varepsilon_i - j(\sigma_i/\omega)$ stands for the complex permittivity of a lossy dielectric in which ε_i and σ_i denote the permittivity and electrical conductivity of each medium, respectively, and j is the imaginary number.

The liquid suspension has a conductivity and permittivity of 4×10^{-4} S/m and $80\varepsilon_0$, respectively. Here, $\varepsilon_0 = 8.85 \times 10^{-12}$ F/m is the vacuum permittivity. The conductivity of the 10 nm gold nanoparticle used in our experiments is considered to be 0.01 S/m as compared to 10^7 S/m for the bulk gold as a result of the surface coating of a layer of chemical stabilization reagent.[22] This matching of particle and liquid electric properties results in a Maxwell−Wagner relaxation frequency of about 2 MHz, as shown in Figure 1D. Correspondingly, in our experiment, the assembly of nanoparticle chains fails to occur at driving frequencies beyond 2 MHz because of the occurrence of a transition from positive DEP to negative DEP.

3.2. Double-Layer Charging Effect. Under ac excitation, an EDL is induced around an ideally polarizable metallic surface in contact with an electrolyte. This metal can be either an electrode connecting to a potential signal source or just a floating conductive element. The electric current from the bulk solution charges the double-layer capacitance on the metal surface. The following charge conservation closes the RC boundary condition at the EDL[23]

$$\sigma_f n \nabla V = j\omega C_{DL}(V - V_0) \quad (3)$$

Here, n is a unit vector normal to the metal surface in the outward direction, $C_{DL} = (\varepsilon_f/\lambda_{Debye})$ is the diffuse layer capacitance in the Debye−Huckel approximation, and λ_{Debye} is the Debye length characterizing the double-layer thickness and is set to 30 nm in the EDL modeling. V is the potential just outside the double layer, and V_0 is the potential in the metal material. Therefore, $(V - V_0)$ is the potential drop across the double layer and is also referred to as the zeta potential.

3.3. ACEO and ICEO. The electric field tangential to the metal surface produces force on the induced charge in the diffuse layer, resulting in a slip velocity profile just outside the double layer that sets the fluid bulk into motion.[24] This phenomenon in microfluidics was first discovered by Ramos et al. in the form of ACEO-induced flow over an electrode array.[24] Their work demonstrated that nonlinear electrokinetic phenomena can originate from transient charge induced on an electrode surface. Later, Bazant and Squires pointed out that it is a much more general situation that an electric field acts on its own induced charge at a polarizable surface and defined the term "induced charge electro-osmosis" (ICEO) to depict the underlying physical mechanism.[21] They announced that ICEO flows can take place around any polarizable surface under the influence of a dc or low-frequency ac field, implying that ICEO is not exclusively over microelectrodes whose voltage oscillation is directly controlled by a signal source, as in ACEO. As a consequence, we use ACEO for electroosmosis flow above the electrodes and ICEO for fluid flow around the conductive island in order to discriminate between the two phenomena because they were discovered by different research groups.

The time-averaged slip velocity $\langle \mathbf{u}_{slip} \rangle$ due to electroosmosis in an ac oscillation is derived from the Helmholtz−Smoluchowski formula

$$\langle \mathbf{u}_{slip} \rangle = \frac{\varepsilon_f}{2\eta} \Lambda Re[(V - V_0)\tilde{\mathbf{E}}_t^*] \quad (4)$$

Here η is the fluid dynamic viscosity and equals 10^{-3} Pa·s at 293.15 K for an aqueous solution. Λ denotes the ratio of the potential drop across the diffuse part of the EDL to the total double-layer potential drop and is set to 0.02 in the modeling of electroosmosis flow. $\tilde{\mathbf{E}}_t^*$ is the complex conjugate part of the tangential electric field just outside the EDL.

It should be highlighted that ACEO has a peak velocity frequency around the inverse RC time scale $f_{RC} = (\sigma_f \lambda_{Debye}/2\pi\varepsilon_f L)$ (L is the characteristic length scale, i.e., the gap size) of the equivalent circuit of the double-layer capacitance in series with the resistor of bulk solution;[24] therefore, the variation in ACEO flow velocity as a function of driving frequency follows a bell-shaped feature. On the contrary, in the case of a floating metal strip in uniform field intensity, ICEO above the metal surface peaks in the dc limit and decays monotonously with increasing frequency.[25] However, things are changed under our experimental conditions, with the simultaneous capacitive charging of the induced EDL at both the electrode and island surface makes ICEO flow above the island surface also a bell-shaped frequency dependence.

3.4. ac Electrothermal Flow. The electrothermal effect arises from dielectric gradients in the fluid bulk. Under such environments, a local charge distribution must be present if the Gauss law and the charge conservation equation are to be satisfied simultaneously. The desired gradients in dielectric constant and conductivity for the occurrence of electrothermal flow often come from anisotropic heating in the bulk fluid due to either Joule heating or externally controlled heat sources. The mean electrothermal body force $\langle \mathbf{f}_{et} \rangle$ averaged over one ac period is given by[26]

$$\langle \mathbf{f}_{et} \rangle = \frac{1}{2} Re\left(\frac{\varepsilon_f(\alpha - \beta)}{1 + j\omega\tau} (\nabla T \cdot \tilde{\mathbf{E}}) \cdot \tilde{\mathbf{E}}^* - \frac{1}{2} \alpha \varepsilon_f (\tilde{\mathbf{E}} \cdot \tilde{\mathbf{E}}^*) \cdot \nabla T \right) \quad (5)$$

Here, T is the temperature distribution in the liquid suspension, and $\tau = \varepsilon/\sigma$ is the charge relaxation time of the solution. α and β are the thermal diffusion coefficients of liquid permittivity and conductivity, respectively.

$$\alpha = \frac{\nabla \varepsilon_f}{\varepsilon_f \nabla T} = -0.004\ \mathrm{K}^{-1} \text{ and } \beta = \frac{\nabla \sigma_f}{\sigma_f \nabla T} = 0.022\ \mathrm{K}^{-1}$$

To obtain the temperature-dependent liquid electric properties, the Fourier heat conduction equation must be solved within the whole DEP device.[27]

$$k\nabla^2 T + \frac{1}{2}\sigma_f(\tilde{\mathbf{E}} \cdot \tilde{\mathbf{E}}^*) = 0 \quad (6)$$

Here, k is the liquid thermal conductivity and equals 0.6 W/(m·K) for water, and $^1/_2\sigma_f(\tilde{\mathbf{E}} \cdot \tilde{\mathbf{E}}^*)$ is a source term caused by Joule heating.

The governing equation for an ac electric field in the sinusoidal steady state obeys the charge conservation in the following form

$$\nabla \cdot ((\sigma + j\omega\varepsilon)\tilde{\mathbf{E}}) = 0 \quad (7)$$

Once the electric field (eq 7) and temperature distribution (eq 6) are evaluated, the electrothermal body force (eq 5) is introduced into the steady-state Navier−Stokes equation for an

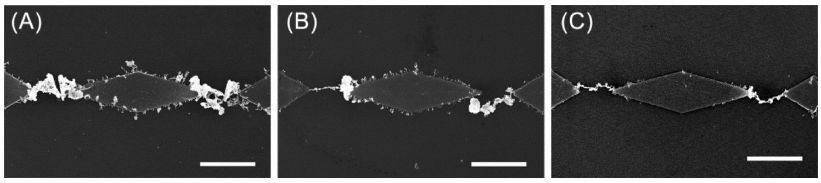

Figure 2. Scanning electron microscopy characterization of DEP-directed superassembly of a 10 nm gold nanoparticle at (A) 50, (B) 150, and (C) 500 kHz. Scale bars are 20 μm in length.

incompressible fluid at a low Reynolds number as a source term of electrical origin.[28]

$$-\nabla p + \nabla\cdot[\eta(\nabla\mathbf{u} + (\nabla\mathbf{u})^{\mathrm{T}})] + \langle\mathbf{f}_{\mathrm{et}}\rangle = 0 \quad (8)$$

Together with the condition of mass conservation, $\bigtriangledown\cdot\boldsymbol{u} = 0$.

Here, p is the hydraulic pressure, and $\mathbf{u}$ denotes the flow velocity vector.

It is worth noting that the first and second terms on the right-hand side of eq 5 denote the Coulomb force and dielectric force, respectively, which act on the fluid volume in opposite directions. If we let eq 5 equal zero, then a critical crossover frequency is found around

$$f_{\mathrm{crossover}} = \frac{\sigma_{\mathrm{f}}}{2\pi\varepsilon_{\mathrm{f}}}\sqrt{1 - \frac{2\beta}{\alpha}} \approx \frac{\sqrt{11}\,\sigma_{\mathrm{f}}}{2\pi\varepsilon_{\mathrm{f}}} = 298\ \mathrm{kHz} \quad (9)$$

The behavior of electrothermal induced flow is dominated by the Coulomb force in the low-frequency range, and the transition to dielectric force takes place at $f_{\mathrm{crossover}}$, where flow reversal occurs.

3.5. Numerical Simulation. To make calculations of the particle DEP velocity, electroosmosis flow, and electrothermal flow, a set of physical equations involving the potential distribution, thermal diffusion, and fluid dynamics must be solved. In this study, a direct numerical simulation based on Comsol Multiphysics 4.3a (a commercial software package that implements a finite element method) is applied to reconstruct the various ICEK phenomena. The computational domain of numerical modeling is shown in Figure 1C.

The complex electric field (eq 7) needs to be solved in the fluid domain as well as the island entity, which has a conductivity of 10^7 S/m. To account for the capacitance skin due to EDL at the metal/electrolyte interface, we directly take into consideration the RC boundary condition (eq 3) on the metal surfaces in the course of the simulation. (a) $\sigma_{\mathrm{f}}\mathbf{n}\cdot\bigtriangledown V = j\omega C_{\mathrm{DL}}(V - V_{\mathrm{app}})$ is imposed on the electrode surface. Here, V_{app} is the potential amplitude applied to the electrodes by an external signal source and prescribed as 10 and 0 V for one electrode and another, respectively. (b) $\sigma_{\mathrm{f}}\mathbf{n}\cdot\bigtriangledown V = j\omega C_{\mathrm{DL}}(V - V_0)$ is imposed on the island surface. V_0 is the potential in the island, which can be determined self-consistently by charge conservation. (c) The condition of zero normal voltage flux $\mathbf{n}\cdot\bigtriangledown V = 0$ is considered on all of the insulation surfaces.

Once the electric field is resolved, the particle DEP velocity $\mathbf{v}_{\mathrm{DEP}}$ can be directly determined using the following relation.

$$\mathbf{v}_{\mathrm{DEP}} = \frac{\langle\mathbf{F}_{\mathrm{DEP}}\rangle}{6\pi\eta R} = \frac{\varepsilon_{\mathrm{f}}R^2 Re[f_{\mathrm{CM}}(\omega)]\nabla(\tilde{\mathbf{E}}\cdot\tilde{\mathbf{E}}^*)}{6\eta} \quad (10)$$

As shown in Figure 1C, the temperature field (eq 6) needs to be solved for the entire DEP device, including the fluid bulk and the silicon substrate (k_{Si} = 140(W/m·K)) of 500 μm thickness. The gold electrodes are considered to be transparent for transferring the heat flux due to their submicrometer thickness. (a) Ambient temperature T = 293.15 K is fixed on the bottom of the substrate. (b) Adiabatic condition $\mathbf{n}\cdot\bigtriangledown T = 0$ is imposed on the external surfaces of the liquid droplet and silicon substrate. (c) The continuity of the conductive heat flux and temperature on the inner walls of the DEP device is applied to conjugate the heat transfer between the substrate and the liquid.

For the modeling of electroosmosis flow, the Navier−Stokes equation in the absence of any bulk force is solved in the fluid domain and simultaneously subjected to (a) the slip velocity function eq 4 at the metal surfaces and (b) a no-slip wall boundary condition at all the insulation surfaces.

As for the modeling of ac electrothermal flow, eq 8 in the presence of the source term is calculated and subjected to a no-slip wall boundary condition at all of the interfaces.

4. RESULTS AND DISCUSSION

4.1. Experimental Results. From Figure 2, nanoparticle chains become thinner and better-shaped with increasing frequency from 50 to 500 kHz.

The nanoparticle wires bridging the conductive objects are rather rambling and thick at 50 kHz (Figure 2A), and they extend a short distance onto the conductive surfaces beyond the metal tips, where the electric field is most intensive from intuition. Simultaneously, the attachment of an abundance of particle clusters to the island edges takes place under this condition.

A further increase in driving frequency to 150 kHz makes the central part of these microwires thinner in the gap regions, but they remain thick adjacent to the conductive tips (Figure 2B). Highly oriented nanoparticle nanowires aligned along the shortest distance of the conductive objects are achieved at 500 kHz and end just at the metal tips (Figure 2C).

Besides, at low frequencies such as 50 and 150 kHz, wire-shaped particle clusters aligned along the direction of local field lines tend to accumulate at the metal edges, and they are more densely and regularly distributed along the island rims as compared to growing from the electrode edges. However, at high driving frequency such as 500 kHz, few nanoparticle aggregates are embedded in the island edges.

4.2. Double-Layer Charging Effect on DEP Force Distribution. The ions in the electrolyte bulk are driven by an applied voltage signal and accumulate at the metal surface. The electrical current from the bulk solution charges the double-layer capacitance at the metal/electrolyte interface.[29] At low frequencies $f \ll f_{\mathrm{RC}} = (\sigma_{\mathrm{f}}\lambda_{\mathrm{Debye}}/2\pi\varepsilon_{\mathrm{f}}L)$, the counterionic cloud on the metal surface fully screens the electric field generated from the electrode; therefore, most of the applied potential difference drops across the capacitive double layers. With an increase in driving frequency such as $f \gg f_{\mathrm{RC}}$, it is extraordinarily difficult for the diffuse layer charge to follow instantaneously the alternation of the harmonic varying signal

dx.doi.org/10.1021/la402060g | Langmuir 2013, 29, 12093−12103

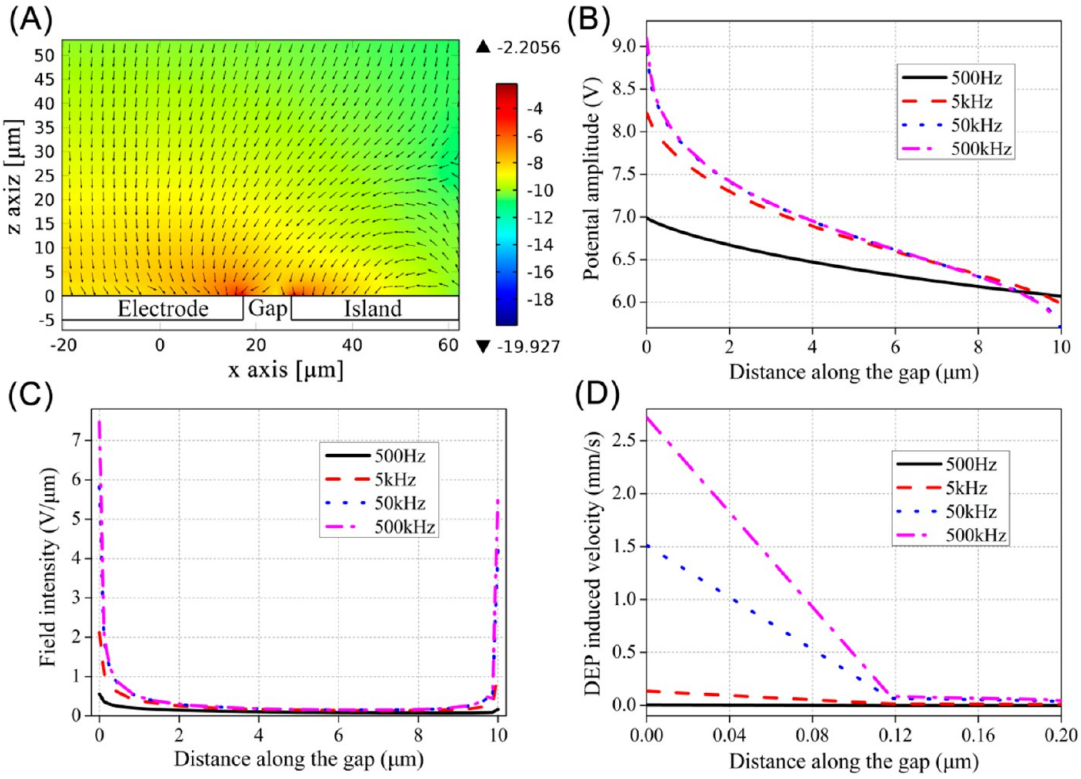

Figure 3. Illustration of the double-layer charging effect on the DEP force: (A) particle DEP velocity in CS1 at 50 kHz (color plotted on the log scale, units 10^x m/s). (B) Distribution of potential amplitude along the gap centerline that connects the opposing tips of one electrode and the island. (C) Field intensity along the gap centerline. (D) Particle DEP velocity along the gap centerline within a short horizontal distance from the electrode tip.

due to a relaxation process, which results in an incomplete formation of EDL.

From Figure 3A, despite the EDL charging effect at 50 kHz, nanoparticles still experience a positive DEP force that attracts them to the vicinity of the metal tips. The zeta potential of the induced double layers is still not negligibly small at 50 kHz as compared to that at 500 kHz (Figure 3B). Consequently, the field intensity extends more efficiently into the bulk solution at a rather high frequency of 500 kHz. On the contrary, the penetration of the electric field into the electrolyte solution is considerably inhibited below 100 kHz as a result of the capacitive charging of EDL on all metal surfaces (Figure 3C).

According to eq 1, the DEP force is proportional to the field intensity squared. Because it attenuates exponentially with the distance from the powering electrodes, we merely exhibit the distribution of the particle DEP velocity at a length of 0.2 μm (Figure 3D). It is worth noting that the DEP force is dependent on the driving frequency as a result of the advent of EDL, in addition to the contribution from the CM factor. The DEP force is even intensified 2-fold with increasing frequency from 50 to 500 kHz. One plausible reason that accounts for non-negligible double-layer charging even above 50 kHz is partially the idealized triangle-shaped solid tips adopted for both the electrode pair and the conductive island in our simulation, resulting in excessive electrode polarization at these geometric asperities. As a consequence, it is necessary to utilize a driving frequency as high as 500 kHz to obtain sufficient DEP driving force to achieve the controlled assembly of highly oriented thin nanoparticle nanowires (Figure 2C).

4.3. ACEO and ICEO. The tangential component of the electric field vector produces force on the diffuse layer charge that sets the fluid in motion. The slip velocity due to the induced zeta potential across the EDL activates ACEO over the electrode surface as well as ICEO adjacent to the conductive island.

The specific circulating fluid rolls induced by electroosmosis at 50 kHz are shown in Figure 4A. Two large flow vortices are produced by the electrode pair connected to a harmonic potential difference through the ACEO mechanism, accompanied by two smaller convective rolls over the island surface arising from ICEO. These flows stream downward over the gap center, sweep across the metal surfaces outward on the electrode or inward to meet one another at the center of the island surface, and then go upward to form circulating fluid flow patterns. From Figure 4B, the transportation of nanoparticle populations from the two sides to the gap region is accelerated to some extent by the streamlines of electroosmosis flow, which in turn makes the assembled nanoparticle wires much thicker in the low-frequency range (Figure 2A,B).

To get a better understanding of the electroosmosis flow effect on particle DEP motion, a further comparison of these two forces is imperative. Figure 4C,D exhibits the magnitude of particle velocity components induced by these two forces on the metal surfaces at 50 kHz. It is quite interesting that the DEP force peaks not just at the metal tips but instead on the metal surfaces within a minor horizontal distance from the solid tips, which can be explained by the excessive electrode polarization at these geometrical asperities. In fact, this exceptional discovery in simulation is in excellent agreement with the experimental observation that the ends of nanoparticle chains always tend to extend a short distance onto the conductive surfaces at 50 kHz (Figure 2A).

dx.doi.org/10.1021/la402060g | *Langmuir* 2013, 29, 12093−12103

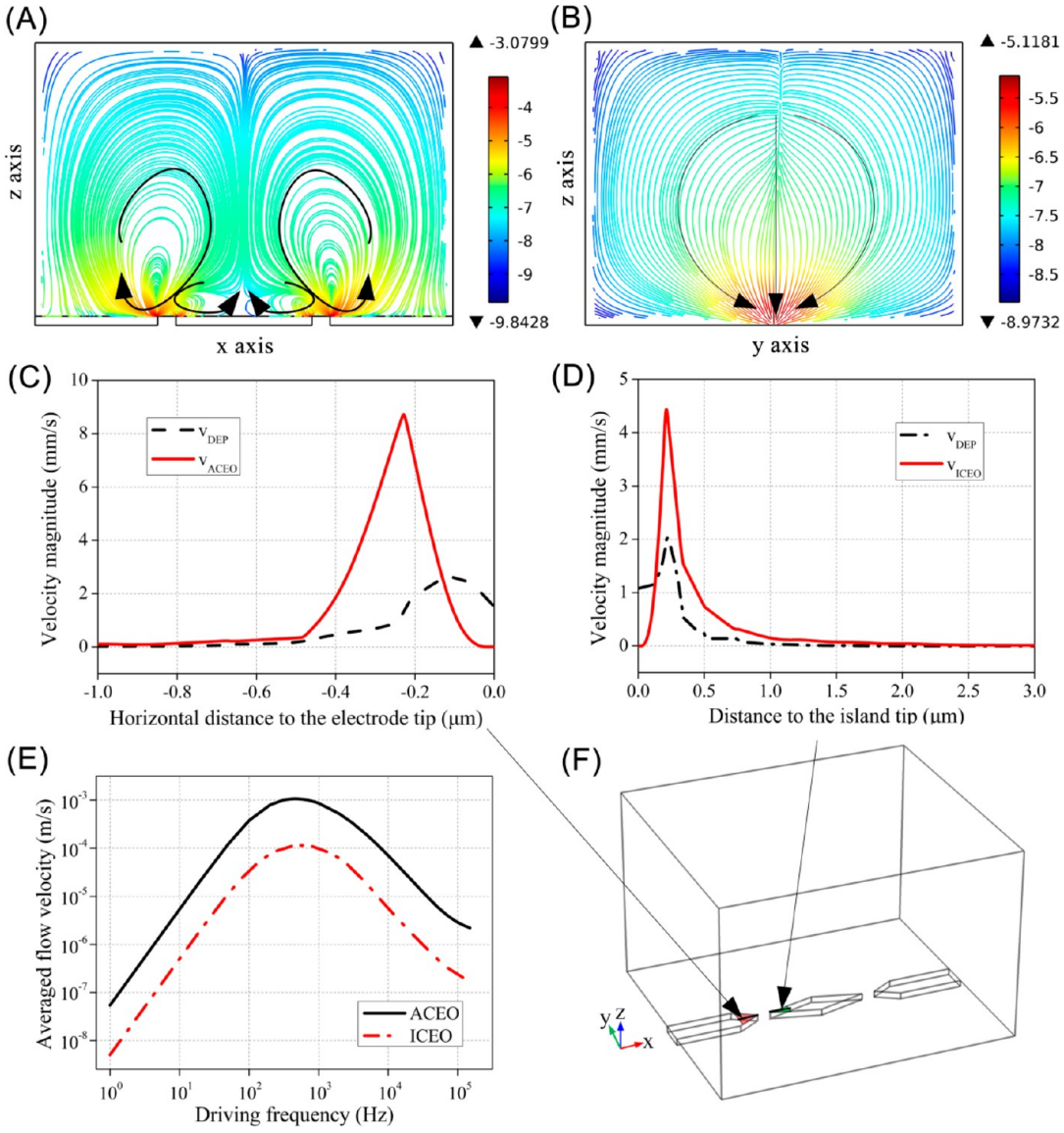

Figure 4. Illustration of ACEO and ICEO fluid flow effects on the DEP assembly of gold nanoparticles in our conductive-island-based microelectrode system. (A) Streamline and arrow plot of electroosmosis flow in CS1 (color plotted on a log scale, units 10^x m/s). (B) Streamline and arrow plot of electroosmosis flow in CS2 at 50 kHz (color plotted on a log scale, units 10^x m/s). (C) Competition of ACEO flow with particle DEP velocity on the electrode centerline as a function of distance from the electrode tip at 50 kHz. (D) Competition of ICEO flow with particle DEP velocity on the island centerline as a function of distance from the island tip at 50 kHz. (E) Comparison of the magnitude of ACEO flow on the electrode surface with that of ICEO flow at the island/electrolyte interface as a function of driving frequency. (F) Surface area used to evaluate the mean electroosmosis flow velocity (red region for ACEO and green region for ICEO).

Electroosmosis flow approaches zero velocity at the metal tips as a result of the no-slip wall boundary condition defined on the surface of the silicon substrate and peaks on the metal surfaces a distance of 0.22 μm from the tips (Figure 4C,D). Although the DEP force helps to attract nanoparticles to the metal surfaces (Figure 3A), electroosmosis flow tends to levitate particles upward into the bulk solution (Figure 4A). The counteraction of these two force components makes it almost impossible for any individual particle to collect on the metal surfaces at low driving frequencies because electroosmosis flow dominates the attractive DEP motion in most regions (Figure 4C,D). As a result, in the low-frequency range where electroosmosis flow plays a nontrivial role in DEP assembly, neighboring particles should at first attract one another in the bulk solution by mutual DEP to form local particle aggregates of a larger diameter. These particle aggregates are then transported to the vicinity of the metal surfaces by electroosmosis flow and finally are captured by an enhanced near-field DEP effect due to the enlarged particle volume so as to form stable assembly patterns (Figure 2A,B).

A parametric study is then conducted to interrogate the frequency dependence of both ACEO and ICEO fluid flows, as shown in Figure 4E. ICEO flow velocity above the island surface exhibits a bell-shaped frequency dependence, the same as that for ACEO flow above the electrode surface. This phenomenon is different from the conventional theoretical prediction for ICEO that peaks in the dc limit and decays monotonically with driving frequency.[25] Simultaneous double-layer charging on the surface of both the electrode pair and the island is responsible for this specific observation. The complete electrode polarization at frequencies well below the inverse RC time scale diminishes the electric field tangential to the island

dx.doi.org/10.1021/la402060g | *Langmuir* 2013, 29, 12093−12103

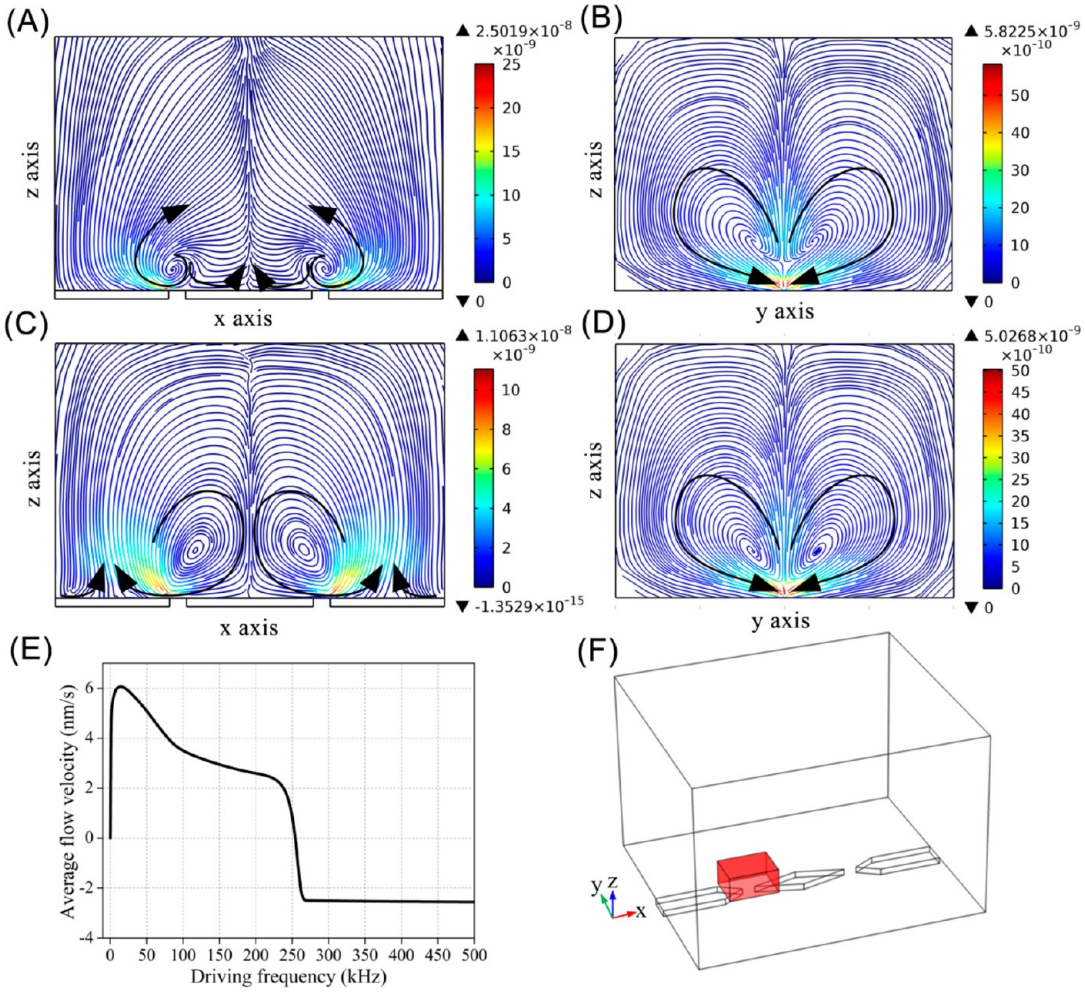

Figure 5. Illustration of the ac electrothermal flow effect on the DEP assembly of gold nanoparticles in the conductive-island-based microelectrode system: (A) electrothermal flow in CS1 at 150 kHz (units m/s); (B) electrothermal flow in CS2 at 150 kHz (units m/s); (C) electrothermal flow in CS1 at 500 kHz (units m/s); (D) electrothermal flow in CS2 at 500 kHz (units m/s); (E) averaged electrothermal flow velocity as a function of driving frequency; and (F) illustration of the specific volume used to evaluate the mean electrothermal flow velocity.

surface, resulting in a negligible slip velocity contribution. At sufficiently high driving frequencies, a relaxation process inhibits free charge from accumulating at the surface, leading to an incomplete formation of EDL. Though the two kinds of electroosmosis flow, both peak at about 500 Hz (Figure 4E), and the ICEO fluid flow has a velocity about 1 order of magnitude smaller than that of ACEO flow, which is directly produced from the electrode surfaces. However, because the DEP force is weakened on the island surface (Figure 4C,D), the influence of ICEO flow on DEP assembly ought to be taken into account as well.

As analyzed previously, particles are transported by electroosmosis flow into the vicinity of the metal structure and then are captured by a strong DEP trapping force at the metal edges. However, because ACEO is about 10 times stronger than ICEO, it may sweep the nanoparticles too quickly across the electrode surface to let them settle down the electrode edge. On the contrary, ICEO flow above the conductive island is much slower than ACEO flow on the electrode, and as a consequence, ICEO can leave enough time for the DEP trapping force to capture the nanoparticles on the island edge.

Consequently, particle clusters tend to accumulate at the island edges rather than at the electrode rims, which is in good agreement with Figure 2A,B, where the wire-shaped nanoparticle clusters aligned along the direction of local field lines are more regularly and abundantly distributed at the island edges, but few particle clusters are collected on the electrode edges as a result of an unduly sweeping effect of ACEO above the electrode surfaces.

4.4. ac Electrothermal Flow. In addition to these aforementioned surface flows, fluid flows originating directly from the active force in the bulk solution are also possible through the induction EHD mechanism. In typical microsystems, induction EHD often appears in the form of ac electrothermal flow. Gradients in the liquid conductivity and dielectric constant due to anisotropic heating in the solution interact with an applied electrical field, inducing a local free charge distribution that follows the field vector with a certain spatial phase lag.[26,30] The collision of these charged ions with other electroneutral molecules in the solution imparts momentum to their surrounding fluid and, as a consequence, drives the electrothermal induced flow.

We use DI water for particle dispersion, which causes trivial electric heat generation. However, because the DEP force on nanosized materials is severely suppressed by their extraordinarily small volume, fluid flow due to electrothermal force can be comparable to the DEP-induced velocity within a certain

dx.doi.org/10.1021/la402060g | Langmuir 2013, 29, 12093−12103

distance from the electrode plane. Consequently, it is necessary to investigate the electrothermal effect on PCF assembly.

At 150 kHz, two large counter-rotating convective vortices dominate the global flow behavior above the electrode pair (Figure 5A). Meanwhile, two local fluid rolls also appear above the island surface as a result of the concentration of Joule medium heating near the island edges, and they meet at the center of the island surface. The fluid movement becomes zero there because of flows from opposite directions, and as a result, a stagnation line for particle collection is created in the center of the island.

At 500 kHz, the most striking feature of the electrothermal effect is the occurrence of flow reversal (Figure 5C). Instead of levitating upward in the low-frequency range, the fluid rolls are dashing downward above the center of the island at such a high frequency, which no longer permits the existence of the stagnation line for particle collection. In addition, unlike electroosmosis effect (Figure 4B), streamlines of electrothermal flow exhibit circulation patterns even in the assembly region (Figure 5B,D), resulting in a mitigation of nanoparticle transportation to the growing microwires from the two sides as compared to electroosmosis flow.

The charging effect of the double-layer capacitance at the metal/electrolyte interface is taken into account as well in the modeling of the electrothermal flow. Figure 5E is an illustration of the frequency dependence of the electrothermal flow velocity. Though the saturation of the Coulomb force at low driving frequency is well predicted by the theory of in-phase electrothermal streaming as in our case,[31] the excessive electrode polarization makes the electrothermal body force invalid at these low frequencies. A compromise between the two effects leads to the fact that electrothermal flow peaks at a single characteristic frequency of around 20 kHz (Figure 5E).

From Figure 5E, the exact crossover frequency of flow reversal in our situation is $f_{crossover}$ = 250 kHz rather than 298 kHz as predicted from eq 9. In fact, eq 9 is obtained in the idealized case where $\tilde{\mathbf{E}}$ is purely real and ∇T is parallel to $\tilde{\mathbf{E}}$. However, actually, $\tilde{\mathbf{E}}$ is complex and ∇T is not parallel to $\mathbf{E}$ in our 3D experimental model, so a direct numerical simulation is advantageous in making a calculation of the ac electrothermal flow and predicting $f_{crossover}$.

With a further increases of frequency beyond $f_{crossover}$, the fluid behavior remains rather stable in that the dielectric force is independent of frequency with the approximation of small temperature gradients.[31]

4.5. Mutual Dielectrophoresis. The electrostatic interaction of neighboring particles due to an electrical near-field effect becomes evident once they approach one another.[32] In this section, the DEP mutual chaining force and repelling force between neighboring particles are investigated as important factors that affect the formation of nanoparticle chains.

In the presence of any near-field effect, the time-averaged DEP force acting on a particle can be obtained through a surface integral of a Maxwell stress tensor (MST) at the particle−fluid interface[33]

$$\langle \mathbf{F}_{dep} \rangle = \oint_{\partial P} \left[\frac{Re(\tilde{\varepsilon}_f)}{4} (\tilde{\mathbf{E}}_f \tilde{\mathbf{E}}_f^{*} + \tilde{\mathbf{E}}_f^{*} \tilde{\mathbf{E}}_f - |\tilde{\mathbf{E}}_f|^2 \cdot I) \cdot n \right] dS \tag{11}$$

Here, ∂P represents the surface of the particle, I is a unit tensor, $\tilde{\mathbf{E}}_f$ is the electric field obtained in the fluid region along the particle surface, and n is the unit vector normal to the particle surface in the outward direction.

First and foremost, we focus on the chaining force of neighboring particles. The parallel arrangement mode of two neighboring gold nanoparticles is shown in Figure 6. Particle 1

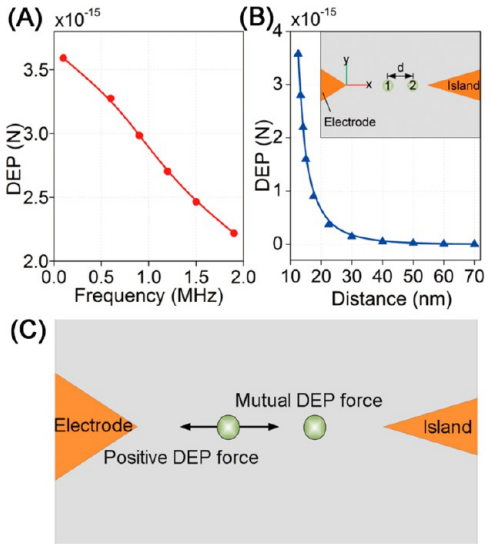

Figure 6. Mutual DEP force along the x axis between two closely positioned particles aligned with their connecting line parallel to the local electric field lines. (A) DEP force acting on particle 1 as a function of frequency while the distance of particle centers is kept at 2.5R. (B) DEP force acting on particle 1 as a function of the particle center-to-center distance at 150 kHz. (C) Illustration of two DEP force components acting on the left particle.

is fixed at a horizontal distance of 1.2 μm from the electrode tip, and particle 2 with their connecting line parallel to the horizontal direction moves away from particle 1.

As shown in Figure 6A, the chaining force decreases gradually with increasing frequency, and no characteristic frequency of the zero chaining force can be found, which seemingly violates the chaining force formulation proposed in ref 18. According to the $Re|K(\omega)|^2$ term in this equation, the chaining force should crossover zero around the interfacial relaxation frequency, which is favorable for many scientists who want to manipulate nanoparticles individually. In fact, the premise of an accurate prediction of the DEP interaction using this formula is that the distance between nanoparticles is much larger than their diameter. It is therefore imperative to utilize the MST approach to make a calculation of the DEP interaction force once the nanoparticles are closely packed. The combinational effect of a suppressed positive DEP force and a weakened attractive chaining force may serve as a plausible explanation for a lowered assembly rate with increasing frequency.

In Figure 6B at 150 kHz, the attractive chaining force drops abruptly at a particle distance of 30 nm and loses its effect once beyond 70 nm. In fact, the result of MST integration is a superposition of two force components, including the positive DEP force and mutual DEP force, as shown in Figure 6C. On one hand, positive DEP is due to the background field gradient created by the voltage signal applied to the electrodes. On the other hand, mutual DEP is derived from the field nonuniformity resulting from the presence of any neighboring particle. The two force components acting on the left particle point in opposite directions, with positive DEP attracting it to

dx.doi.org/10.1021/la402060g | Langmuir 2013, 29, 12093−12103

the electrode tip while mutual DEP pulls it to the right particle. Though the positive DEP force is independent of the particle distance, mutual DEP is a decreasing function of the particle center-to-center distance. As shown in Figure 6B, mutual DEP dominates the behavior of particle 1 within a particle distance of 70 nm, and particle chaining can take place under this condition. However, for a particle distance beyond 70 nm, the resultant force on the left particle becomes a negative value, implying that positive DEP has overwhelmed mutual DEP. Consequently, particle 1 is attracted to the electrode tip rather than the right nanoparticle, leading to a failure in the occurrence of direct particle chaining.

A similar analysis is applied to investigate the repulsion behaviors of neighboring particles with their connecting line perpendicular to the local electric field lines (Figure 7). The

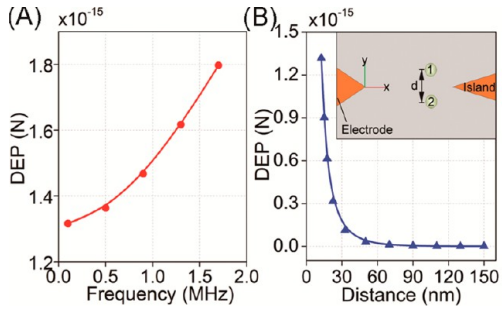

Figure 7. Repulsive mutual DEP force along the *y* axis between two adjacent particles aligned with their connecting line perpendicular to the local electric field lines. (A) DEP force acting on particle 1 as a function of frequency while the distance between particle centers is kept at 2.5*R*. (B) DEP force acting on particle 1 as a function of the particle center-to-center distance at 150 kHz.

frequency dependence of the mutual repelling DEP force at a particle distance of 2.5*R* is shown in Figure 7A. The repelling force is an increasing function of the driving frequency, which can account for the fact that gold nanoparticle chains tend to become thinner at high frequency from a new perspective, in comparison to the conventional consideration of decreasing ACEO flow velocity with frequency.

From Figure 7B, similar to the attractive chaining force, the repelling DEP force is a decreasing function of the particle center-to-center distance as well. However, the repelling force acting on an individual particle falls more slowly with particle distance as compared to the chaining force. This kind of repelling force still plays a dominant role in particle behavior against the positive DEP force as the particle distance approaches 150 nm. On the contrary, the chaining force around the same area loses its dominant effect once the particle distance is merely beyond 70 nm. However, in spite of its smaller effective length scale, the chaining force is about 3 times larger than the repelling force under the influence of an identical background field intensity.

4.6. Combinational Effects of Various ICEK Phenomena. Figure 6 illustrates the electrokinetic behavior of an individual nanoparticle due to the combinational effects of various ICEK phenomena at three typical driving frequencies corresponding to the experimental results shown in Figure 2.

At 50 kHz, double-layer charging makes electroosmosis flow the most dominant ac force that transports nanoparticles onto the metal structures, and the DEP force has been considerably restricted as indicated by those nearly horizontal arrows around the metal tips in Figure 8A.

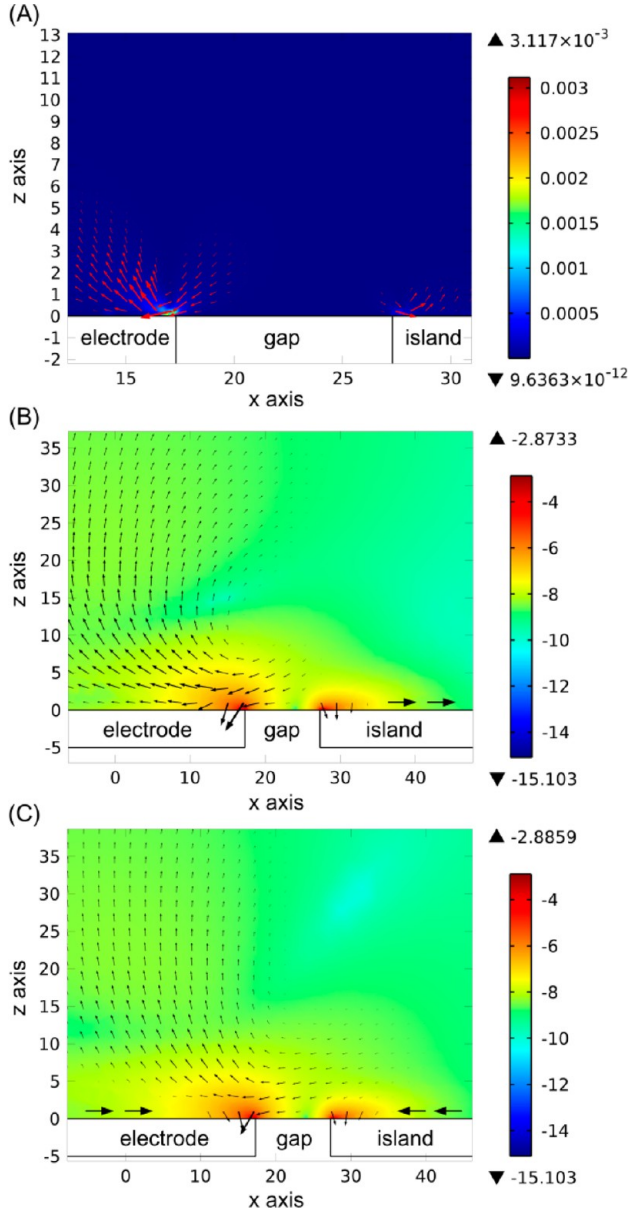

Figure 8. Particle motion due to the combinational effects of various ICEK phenomena in CS1: (A) particle velocity due to electroosmosis flow and DEP force at 50 kHz (units m/s); (B) particle velocity due to the Coulomb force component of electrothermal flow and the DEP effect at 150 kHz (color plotted on the log scale, units 10^x m/s); (C) particle velocity due to the dielectric force component of electrothermal flow and DEP effect at 500 kHz (color plotted on the log scale, units 10^x m/s).

At 150 kHz, though electroosmosis flow diminishes because of the relaxation process, the Coulomb force acting on the spatial residual charge actuates the electrothermal flow in the bulk solution. Electrothermal flow helps to transport nanoparticles from the far-field region to the vicinity of the metal structure, and then they are finally captured by the strong DEP trapping force at the metal tips, as indicated by the nearly vertical arrows in Figure 8B.

dx.doi.org/10.1021/la402060g | *Langmuir* 2013, 29, 12093−12103

At 500 kHz, the particle dynamics is identical to that at 150 kHz, whereas the direction of fluid motion above the metal surfaces has been reversed by the action of the dielectric force (Figure 8C).

5. CONCLUSIONS

In this study, on the basis of the DEP mechanism, the controlled assembly of 10 nm gold nanoparticles into microwire electrical connections is demonstrated experimentally in a conductive-island-based microelectrode system. At 50 kHz, the ends of nanoparticle chains are extended onto the electrode/island surfaces a short distance from the metal tips. At 150 kHz, nanoparticle chains become thinner around the gap center but are still rather thick and rambling at the metal tips. With a further increase of frequency to 500 kHz, highly oriented nanoparticle nanowires of a uniform minimal thickness are produced by DEP. Besides, in the low-frequency range, wire-shaped particle clusters are densely and regularly distributed along the island edges, but few are collected on the electrode rims.

To account for these regular experimental results, we have introduced here the theory of ICEK phenomena. The advent of EDL not only weakens the magnitude of the DEP force in the solution bulk but also shifts the DEP maximum a step further onto the metal surfaces beyond the solid tips as a result of the excessive electrode polarization at these geometrical asperities. ICEO flow vortices above the conductive island are superimposed with a background ACEO flow produced from the electrode surfaces, which can help to transport plenty of particle populations to the gap region, thickening the assembled particle chains at low frequencies. As observed in experiments, a fast ACEO flow may sweep the nanoparticles too quickly across the electrode surface to let them settle down safely on the electrode edge. In contrast, the moderate magnitude of ICEO flow velocity can leave enough time for the DEP trapping force to capture nanoparticles on the island edges, resulting in a collection of abundant particle clusters along the island rims. Besides, flow patterns due to electrothermal force in a range of frequencies are investigated as well. A stagnation line for particle collection is created at the center of the island surface below a crossover frequency but vanishes at high driving frequencies as a result of the transition of fluid behavior from being Coulomb force dominated to being dielectric force dominated. In addition, because of an electrical near-field effect, the particle concentration also exerts a significant influence on the PCF assembly through mutual DEP. These results provide valuable insight into the controlled assembly of on-chip microwire electrical connections from colloidal suspensions.

AUTHOR INFORMATION

Corresponding Author

*E-mail: jyshao@mail.xjtu.edu.cn.

Author Contributions

H.D. and W.L. contributed equally.

Notes

The authors declare no competing financial interest.

ACKNOWLEDGMENTS

This research was mainly supported by the Major Research Plan of NSFC on Nanomanufacturing under grant no. 90923040, the National Basic Research Program of China under grant no. 2009CB724202, the NSFC projects under grant nos. 51005178 and 51275401.

REFERENCES

(1) Jones, T. B. *Electromechanics of Particles*; Cambridge University Press: New York, 1995.

(2) Hermanson, K. D.; Lumsdon, S. O.; Williams, J. P.; Kaler, E. W.; Velev, O. D. Dielectrophoretic Assembly of Electrically Functional Microwires from Nanoparticle Suspensions. *Science* **2001**, *294*, 1082−1086.

(3) Khondaker, S. I.; Yao, Z. Fabrication of Nanometer-Spaced Electrodes Using Gold Nanoparticles. *Appl. Phys. Lett.* **2002**, *81*, 4613−4615.

(4) Barsotti, R. J., Jr.; Vahey, M. D.; Wartena, R.; Chiang, Y. M.; Voldman, J.; Stellacci, F. Assembly of Metal Nanoparticles into Nanogaps. *Small* **2007**, *3*, 488−499.

(5) Cheon, D.; Kumar, S.; Kim, G.-H. Assembly of Gold Nanoparticles of Different Diameters between Nanogap Electrodes. *Appl. Phys. Lett.* **2010**, *96*, 013101.

(6) Gierhart, B. C.; Howitt, D. G.; Chen, S. J.; Smith, R. L.; Collins, S. D. Frequency Dependence of Gold Nanoparticle Superassembly by Dielectrophoresis. *Langmuir* **2007**, *23*, 12450−12456.

(7) Kretschmer, R.; Fritzsche, W. Pearl Chain Formation of Nanoparticles in Microelectrode Gaps by Dielectrophoresis. *Langmuir* **2004**, *26*, 11797−11801.

(8) Bezryadin, A.; Dekker, C.; Schmid, G. Electrostatic Trapping of Single Conducting Nanoparticles between Nanoelectrodes. *Appl. Phys. Lett.* **1997**, *71*, 1273−1275.

(9) Papadakis, S. J.; Gu, Z.; Gracias, D. H. Dielectrophoretic Assembly of Reversible and Irreversible Metal Nanowire Networks and Vertically Aligned Arrays. *Appl. Phys. Lett.* **2006**, *88*, 233118.

(10) Liu, Y. L.; Chung, J. H.; Liu, W. K.; Ruoff, R. S. Dielectrophoretic Assembly of Nanowires. *J. Phys. Chem. B* **2006**, *110*, 14098−14106.

(11) An, L. B.; Cheam, D. D.; Friedrich, C. R. Controlled Dielectrophoretic Assembly of Multiwalled Carbon Nanotubes. *J. Phys. Chem. C* **2009**, *113*, 37−39.

(12) Xu, D.; Shou, K.; Nelson, B. J. Dielectrophoretic Assembly of Carbon Nanotube-Based NEMS Devices Using Floating Electrodes. *Microelectron. Eng.* **2011**, *88*, 2703−2706.

(13) Tegenfeldt, J. O.; Prinz, C.; Cao, H.; Huang, R. L.; Austin, R. H.; Chou, S. Y.; Cox, E. C.; Sturm, J. C. Micro- and Nanofluidics for DNA Analysis. *Anal. Bioanal. Chem.* **2004**, *378*, 1678−1692.

(14) Vedala, H.; Roy, S.; Doud, M.; Mathee, K.; Hwang, S.; Jeon, M.; Choi, W. The Effect of Environmental Factors on the Electrical Conductivity of a Single Oligo-DNA Molecule Measured Using Single-Walled Carbon Nanotube Nanoelectrodes. *Nanotechnology* **2008**, *19*, 265704.

(15) Taff, B. M.; Voldman, J. A Scalable Addressable Positive-Dielectrophoretic Cell-Sorting Array. *Anal. Chem.* **2005**, *77*, 7976−7983.

(16) Rosenthal, A.; Taff, B. M.; Voldman, J. Quantitative Modeling of Dielectrophoretic Traps. *Lab Chip* **2006**, *6*, 508−515.

(17) Pethig, R. Dielectrophoresis: Using Inhomogeneous AC Electrical Fields to Separate and Manipulate Cells. *Crit. Rev. Biotechnol.* **1996**, *16*, 331−348.

(18) Gupta, S.; Alargova, R. G.; Kilpatrick, P. K.; Velev, O. D. On-Chip Dielectrophoretic Coassembly of Live Cells and Particles into Responsive Biomaterials. *Langmuir* **2010**, *26*, 3441−3452.

(19) Lapizco-Encinas, B. H.; Davalos, R.; Simmons, B. A.; Cummings, E. B.; Fintschenko, Y. An Insulator-Based (Electrodeless) Dielectrophoretic Concentrator for Microbes in Water. *J. Microbiol. Methods* **2005**, *62*, 317−326.

(20) Bhatt, K. H.; Velev, O. D. Control and Modeling of the Dielectrophoretic Assembly of on-Chip Nanoparticle Wires. *Langmuir* **2004**, *20*, 467−476.

(21) Bazant, M. Z.; Squires, T. M. Induced-Charge Electrokinetic Phenomena: Theory and Microfluidic Applications. *Phys. Rev. Lett.* **2004**, *92*, 066101.

(22) Li, M.; Qu, Y.; Dong, Z.; Wang, Y.; Li, W. Limitations of Au Particle Nanoassembly Using Dielectrophoretic Force—A Parametric Experimental and Theoretical Study. *IEEE Trans. Nanotechnol.* **2008**, *7*, 477−479.
(23) García-Sánchez, P.; Ren, Y. K.; Arcenegui, J. J.; Morgan, H.; Ramos, A. Alternating Current Electrokinetic Properties of Gold-Coated Microspheres. *Langmuir* **2012**, *28*, 13861−13870.
(24) Green, N. G.; Ramos, A.; González, A.; Morgan, H.; Castellanos, A. Fluid Flow Induced by Nonuniform Ac Electric Fields in Electrolytes on Microelectrodes. III. Observation of Streamlines and Numerical Simulation. *Phys. Rev. E* **2002**, *66*, 026305.
(25) Pascall, A. J.; Squires, T. M. Induced Charge Electroosmosis over Controllably-Contaminated Electrodes. *Phys. Rev. Lett.* **2010**, *104*, 088301.
(26) González, A.; Ramos, A.; Morgan, H.; Green, N. G.; Castellanos, A. Electrothermal Flows Generated by Alternating and Rotating Electric Fields in Microsystems. *J. Fluid Mech.* **2006**, *564*, 415−433.
(27) Perch-Nielsen, I. R.; Green, N. G.; Wolff, A. Numerical Simulation of Travelling Wave Induced Electrothermal Fluid Flow. *J. Phys. D* **2004**, *37*, 2323−2330.
(28) Du, E.; Manoochehri, S. Electrohydrodynamic-Mediated Dielectrophoretic Separation and Transport Based on Asymmetric Electrode Pairs. *Electrophoresis* **2008**, *29*, 5017−5025.
(29) Ramos, A.; Morgan, H.; Green, N. G.; González, A.; Castellanos, A. Pumping of Liquids with Traveling-Wave Electroosmosis. *J. Appl. Phys.* **2005**, *97*, 084906.
(30) Iverson, B. D.; Cremaschi, L.; Garimella, S. V. Effects of Discrete-Electrode Configuration on Traveling-Wave Electrohydrodynamic Pumping. *Microfluid. Nanofluid.* **2009**, *6*, 221−230.
(31) Hong, F. J.; Bai, F.; Cheng, P. Numerical Simulation of AC Electrothermal Micropump Using a Fully Coupled Model. *Microfluid. Nanofluid.* **2012**, *13*, 411−420.
(32) Aubry, N.; Singh, P. Influence of Particle-Particle Interactions and Particles Rotational Motion in Traveling Wave Dielectrophoresis. *Electrophoresis* **2006**, *27*, 703−715.
(33) Rosales, C.; Lim, K. M. Numerical Comparison between Maxwell Stress Method and Equivalent Multipole Approach for Calculation of the Dielectrophoretic Force in Single-Cell Traps. *Electrophoresis* **2005**, *26*, 2057−2065.